Configurable lossless broadband beam splitters for semi-guided waves in integrated silicon photonics

Manfred Hammer, Lena Ebers, and Jens Förstner*

Theoretical Electrical Engineering, Paderborn University, Paderborn, Germany

Abstract: We show that narrow trenches in a high-contrast silicon-photonics slab can act as lossless power dividers for semi-guided waves. Reflectance and transmittance can be easily configured by selecting the trench width. At sufficiently high angles of incidence, the devices are lossless, apart from material attenuation and scattering due to surface roughness. We numerically simulate a series of devices within the full 0-to-1-range of splitting ratios, for semi-guided plane wave incidence as well as for excitation by focused Gaussian wave bundles. Straightforward cascading of the trenches leads to concepts for 1×M-power dividers and a polarization beam splitter.

Keywords: photonics, integrated optics, beam splitter, power divider, polarization beam splitter, oblique propagation of semi-guided waves.

1 Introduction

Optical beam splitters can be counted among the key components of photonic circuitry. One distinguishes power splitters, or power dividers, on the one hand, and polarization splitters on the other hand. In a context of integrated optics, power beam splitters aim at distributing the optical power from an input channel waveguide between two or more outlet channels, mostly for waves of uniform polarization. Manifold variants have been proposed, differing in platform and/or particular purpose. Among the more recent proposals are concepts that rely on specifically tailored (adiabatic, tapered) directional couplers [1–3], on multimode-interference couplers (MMIs) [4], Y-junctions [5], or waveguide gratings [6]. Several of these device types can also be configured as polarization beam splitters [7–11], that direct modes of different polarization to separate waveguide outlets.

With the present proposal we target a type of integrated optical systems that operate with semi-guided waves [12,13]. These are only "vertically" guided by a thin-film slab. Laterally, in the direction in-plane perpendicular to the direction of propagation, the waves are either not confined at all, i.e. are characterized by a unique in-plane wavevector and plane wavefront, or they are formed as focused superpositions of the former, as laterally confined bundles of waves of e.g. Gaussian shape. We shall show in this paper that simple trenches in the guiding slab, as introduced in Fig. 1, can act as lossless power dividers in this regime of semi-guided waves. We look explicitly at structures with high refractive index contrast, as in the standard platforms of silicon photonics [14]. The functioning relies on frustrated total internal reflection [15], hence one might view this as an integrated-optical variant of common macroscopic double-prism (cube) beam splitters [15].

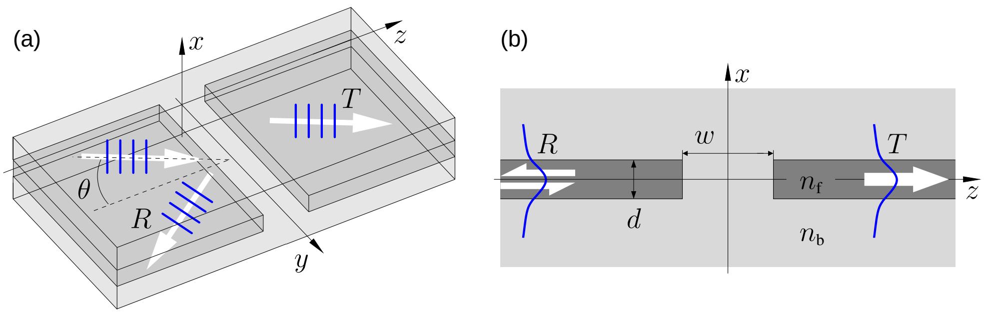

Figure 1: Propagation of semi-guided waves towards a trench in a slab waveguide, schematic (a), and cross section view (b). Cartesian coordinates x, y, z are introduced, with x normal to the slab plane and y parallel to the trench axis. Incoming waves propagate in the y-z-plane at an angle θ with respect to the trench normal, generating outgoing waves with reflectance R and transmittance T. Parameters: refractive indices $n_b = 1.45$ (background), $n_f = 3.45$ (film), slab thickness $d = 0.22\,\mu$m, trench width w, target vacuum wavelength $\lambda = 1.55\,\mu$m.

*Paderborn University, FG Theoretical Electrical Engineering   Warburger Straße 100, 33098 Paderborn, Germany
Phone: ++49(0)5251/60-3560   Fax: ++49(0)5251/60-3524   E-mail: manfred.hammer@uni-paderborn.de

In Section 2 we recapitulate certain more general features of semi-guided waves, and specialize things for the parameters of the present symmetric Si/SiO_2-slabs. Section 3 then takes a look at a single waveguide facet, and its excitation at varying angles of incidence. Trenches of specific width are the subject of Sections 4, 5, where we consider the incidence of laterally unlimited plane waves, and of focused wave bundles, respectively. While the former considerations concern models with trenches of infinite length, in Section 6 we comment on the — rather obvious — practically relevant length restriction. The last two Sections 7, 8 discuss extensions of the single-trench structures, towards power dividers with multiple outlets, and towards a polarization beam splitter. A note on respective concepts for nonsymmetric slabs follows in Appendix A.

2 Oblique propagation of semi-guided waves

Traditional integrated optics of semi-guided waves [16–18] constitutes the primary context for the present paper [12, 13], where our concepts continue a series of more recent proposals on structures with high refractive index contrast. This includes simple mirrors [19], corner- and step-like folds in optical slab waveguides [20–22], coated slab waveguide facets [23, 24], the resonant oblique excitation of channel waveguides with rectangular [25–34] and circular cross sections [35, 36] for the realization of a variety of filtering functions, but also more complex systems like lenses [37], or entire spectrometers [38]. Components operating with semi-guided Bloch surface waves have been discussed as well [39]. Likewise, the devices proposed in this paper are envisioned, in the first place, to be deployed in a framework of photonic circuitry that is based on semi-guided waves, potentially in combination with any of the former components. Clearly, none of these devices, including our beam splitters, are directly compatible with the standard single mode channels ("photonic wires") of silicon photonics. A connection to those would require suitable tapers [19], or e.g. an in-plane grating coupler ("Bragg deflector") [40]. Out-of-chip connections could be realized by gratings for coupling to fibers [41, 42], tailored to the wide semi-guided field, or by direct end-facet coupling with suitable (cylindrical) lenses.

Analysis of our beam splitters starts with a fundamental line of reasoning for systems that are constant along one coordinate axis. In case of the structure of Fig. 1, this is the y-axis parallel to the trench. Half-infinite access waveguides connect to the inner region of interaction. Here, these are the slabs that extend from the central trench in $\pm z$ direction. Incident waves are considered that are confined by one of the slab waveguides, with the functional form of standard plane waves in the in-plane directions, for propagation at an angle θ with respect to the plane normal to y, as indicated in Fig. 1. One arrives at a 2.5-D setting, where the structure is constant along y, but where one looks for solutions of the full vectorial Maxwell equations in the frequency domain, that share the harmonic y-dependence of the incoming semi-guided plane wave.

We refer to [13, 21, 43] for details of this formal analysis, and proceed with a few immediate conclusions for our trench structure. For semi-guided input of a wave with slab-mode effective index N_{in} at angle θ, any output wave governed by an effective index N_{out} propagates at an angle θ_{out} that is related to the angle of incidence by an equation in the form of Snell's law: $N_{\text{out}} \sin\theta_{\text{out}} = N_{\text{in}} \sin\theta$. Hence, in case of the symmetric single-mode slabs, any semi-guided reflected or transmitted waves that are of the same polarization as the input are observed at the same angle $\theta_{\text{out}} = \theta$ as the incident wave.

Any potentially generated non-guided, radiative output waves ("cladding modes") are characterized by effective indices below the background level n_{b}. These become evanescent, if, for semi-guided input with effective index N_{in} at angle θ, no real output angle can be defined, i.e. if $\theta > \theta_{\text{b}}$, for a critical angle θ_{b} with $\sin\theta_{\text{b}} = n_{\text{b}}/N_{\text{in}}$. At vacuum wavelength $\lambda = 1.55\,\mu$m, the slab waveguides of thickness $d = 0.22\,\mu$m with refractive indices $n_{\text{f}} = 3.45$ (core) and $n_{\text{b}} = 1.45$ (substrate and cladding) support fundamental guided slab modes with effective mode indices $N_{\text{TE}} = 2.8227$ and $N_{\text{TM}} = 2.0397$ for TE and TM polarization [44]. One computes respective critical angles $\theta_{\text{b, TE}} = 30.91°$ and $\theta_{\text{b, TM}} = 45.31°$ for TE- and TM-polarized excitation of the trenches. Incidence at angles below these levels can be accompanied by power transfer to non-guided waves; at higher angles all radiative losses are strictly suppressed.

In principle, scattering by the trenches could lead to more or less pronounced polarization conversion [21]. For the present parameters, however, this can be ruled out by symmetry arguments, if one restricts to the lossless regime $\theta > \theta_{\text{b}}$, where only the fundamental slab modes carry power away from the region of interaction. The slab waveguides, and also the entire trench configuration of Fig. 1 are mirror symmetric with respect to the horizontal plane at $x = 0$. For in-plane propagation at arbitrary angles, the vectorial electromagnetic profiles $\boldsymbol{E}$, $\boldsymbol{H}$ of the slab modes [43] are functions of x only. The fundamental TE and TM modes are symmetric in the following way: The TE mode has a profile with $E_x = 0$, even components E_y, E_z, and H_x, and odd components H_y and H_z. For the TM mode, the components E_x, H_y, and H_z are even, and components E_y and E_z are odd, with $H_x = 0$. In the plane $x = 0$ the TE mode thus satisfies what is called perfect magnetic conductor (PMC)-boundary conditions [45], while the TM mode complies with the perfect-electric-conductor (PEC) conditions. These modes thus belong to different symmetry classes; as the full structure is also mirror symmetric with respect to the plane $x = 0$, the symmetry of the incident field transfers to the entire solution. Hence, there is no power transfer ("coupling") between semi-guided waves of different polarization at any of the interfaces, irrespective of the angle of incidence, for $\theta > \theta_b$.

Obviously, the former symmetry arguments require strictly "vertical" trench sidewalls. Fabrication, however, may lead intentionally or unintentionally to trenches with more or less slanted flanks. We briefly comment on this in Appendix A.1.

For the present paper, we rely on a semi-analytical simulation method as described in [43,46,47]. The solver addresses the 2.5-D scattering problem on a two-dimensional rectangular computational domain with transparent-influx boundary conditions. The computational scheme is based on simultaneous expansions into polarized local vectorial slab eigen-modes along the two orthogonal cross section coordinates x, z (vectorial quadridirectional eigenmode propagation vQUEP). The size of the computational domain and the number of expansion terms enter as computational parameters; convergence has been assured as required for the data as displayed.

3 Slab waveguide facets

In preparation of the discussion of the full trench structures, we consider a single waveguide facet first. Fig. 2 shows reflectances R_{TE} and R_{TM} for TE- and TM-polarized excitation of the structure of Fig. 1 for large width w, where the second slab region for $z > 0$ is absent.

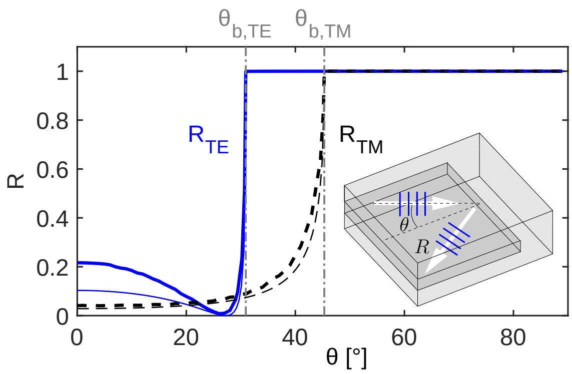

Figure 2: Bold curves: Oblique incidence of polarized semi-guided waves at a single slab facet, reflectances R_{TE} for TE input (continuous), R_{TM} for TM input (dashed) as a function of the incidence angle θ. Thin lines: Reflectances for oblique plane wave incidence at an interface between two dielectric media, for p-polarized waves and refractive index contrast $2.8227 : 1.45$ (continuous) and for s-polarized waves and refractive index contrast $2.0397 : 1.45$ (dashed). Critical angles $\theta_{b,TE}$ and $\theta_{b,TM}$ for radiative losses are indicated.

Unit reflectances are predicted for angles of incidence θ beyond the critical values $\theta_{\text{b,TE}}$, $\theta_{\text{b,TE}}$. Radiative losses vanish in line with our former reasoning; here the facet acts as a perfect mirror. The symmetry arguments from Section 2 apply also to a single facet. For polarized semi-guided input, no power is reflected into the fundamental mode of different polarization. As confirmed by the vQUEP computations (curves are not shown), this holds for the entire range $\theta \in [0, 90[^\circ$ of angles of incidence. In the regions $\theta < \theta_b$, however, the symmetry arguments well permit power transfer to non-guided radiative modes of different polarization and higher order. In that sense, polarization conversion is well possible, but not between the fundamental semi-guided fields that are of interest here.

It is tempting to disregard the vertical wave confinement for a moment, and to view this as a problem of plane wave reflection at a dielectric interface, as predicted by the Fresnel equations [48,49], using the effective indices of the incoming modes as refractive indices. The thin lines in Fig. 2 show the reflectance for p-polarized plane waves at an interface with refractive index contrasts $N_{\text{TE}} : n_b$, and for s-polarized waves with refractive index contrast $N_{\text{TM}} : n_b$, respectively. One observes some qualitative agreement with the vQUEP results for the actual waveguide facets. $\theta_{\text{b,TE}}$, $\theta_{\text{b,TE}}$ indicate the critical angles for total internal reflection in the simplified view. The bold R_{TE}-curve for the facet relates to the TE field with its electric field predominantly parallel to the y-z-plane of incidence. The dip around $\theta = 26^\circ$ can thus be interpreted as a feature akin to the Brewster angle of classical optics. The actual reflectance levels, however, deviate substantially, in particular for near-normal incidence of TE-polarized waves. We will therefore not pursue this effective-index viewpoint any further.

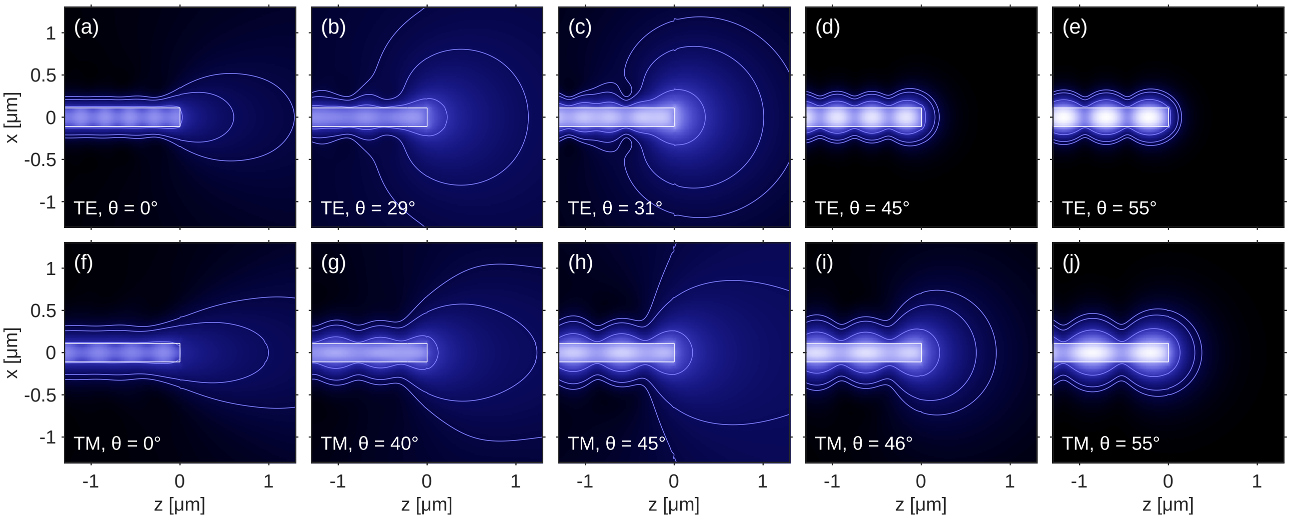

Figure 3: Oblique incidence of semi-guided waves at a slab waveguide facet; energy density u of the optical electromagnetic field on a x-z-plane perpendicular to the facet, for TE (top row) and TM input (bottom row) at angle θ; contour lines at 5%, 1%, and 0.5% of the maximum level, with a uniform color scale for all panels.

Fig. 3 compares a series of field shapes, for polarized excitation of the facets at different angles of incidence. Both polarizations play a role, hence we choose to plot the energy density $u = \mathrm{Re}\,(\epsilon_0 n^2|\boldsymbol{E}|^2 + \mu_0|\boldsymbol{H}|^2)/4$ of the electromagnetic field. The color scale has been adjusted such that also features at low field levels can be recognized. The panels address normal incidence (a, f), incidence close to, below (b, h) and above θ_b (c, i), and incidence at larger angles well beyond the critical angle (d, e, j). Here the gradual decay of the field strength in positive z-direction beyond the facet for $\theta > \theta_\mathrm{b}$ becomes apparent, which will be relevant for the discussion of power dividers in the next sections. That decay rate differs pronouncedly, at the same angle of incidence, for TE- and TM-polarized input (e, j). This will be instrumentalized for the construction of a polarization beam splitter in Section 8.

4 Power dividers

We now consider the full trench structure of Fig. 1. An incidence angle $\theta = 45°$ facilitates simple cascading of beam splitters, with power dividers arranged on a rectangular grid, such as in the example of the $1 \times M$-divider discussed in Section 7. For the present parameters, however, that angle is just below the critical angle $\theta_{\mathrm{b,\,TM}}$ for loss suppression, i.e. not suitable for TM waves, while the polarization beam splitter of Section 8 operates with waves of both polarizations, at the same angle of incidence. Therefore, rather arbitrarily, we select the two angles $45°$ (TE only) and $55°$ (TE and TM) for further evaluation. Reflectances and transmittances as functions of the trench width w, for fixed angle of incidence, are shown in Fig. 4.

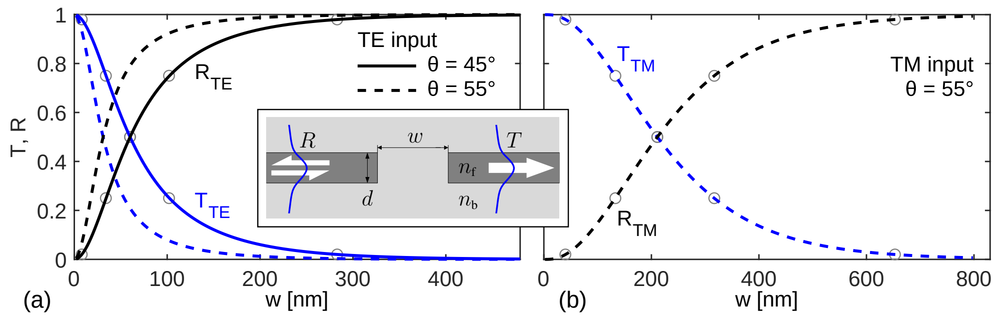

Figure 4: Oblique incidence of semi-guided waves on the trench structure of Fig. 1, reflectance R and transmittance T versus the trench width w; curves for TE (a) and TM excitation (b), at angles $\theta = 45°$ (continuous) and $\theta = 55°$ (dashed). Markers: widths w selected for the further examples in this section.

The curves in Fig. 4 resemble what would be expected for a standard configuration of plane wave reflection at a thin layer with reduced refractive index, if one considers the dependence on the thin-film-thickness for fixed angle on incidence. Tempting though it may be to compare with respective calculations for 1-D multilayers, the quantitative deviations render this not useful in the present context (curves are not shown here). The qualitative agreement, however, points to a mechanism of frustrated total internal reflection (FTIR) [15], here in an essentially 2-D setting.

By construction, the trench structures operate without losses; for each polarization, reflectance and transmittance always add up to one. "Design" of a power divider is then merely a matter of looking up the width w required for any desired reflectance in a diagram such as Fig. 4. Some examples are indicated; the values $w = 0.008, 0.034, 0.060, 0.102, 0.283\,\mu$m (TE) and $w = 0.040, 0.133, 0.211, 0.317, 0.653\,\mu$m (TM) lead to power dividers with a reflectance of $R = 0.02, 0.25, 0.50, 0.75, 0.98$ and transmittance $T = 1 - R$, for angles of incidence $\theta = 45°$ (TE) and $\theta = 55°$ (TM), respectively.

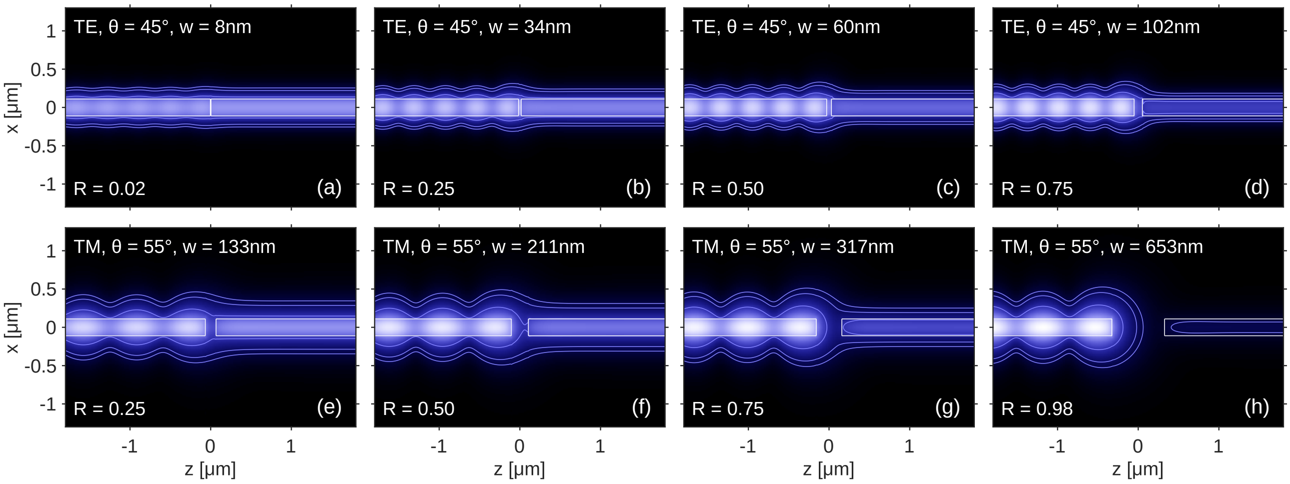

Figure 5: Oblique excitation of trenches of width w at angle θ, TE input (top row), TM input (bottom row); energy density u of the optical electromagnetic field; contour lines at 5%, 1%, and 0.5% of the maximum level, with a uniform color scale for all panel. These are lossless structures with reflectance R and transmittance $T = 1 - R$.

Fig. 5 shows cross-sectional fields for some of these configurations. These can be understood in terms of the FTIR process. According to Fig. 3, the reflection of the incoming wave at the facet on the input side generates a field buildup beyond the facet. The second output facet "taps" into that field, where the field strength at the position of the second facet decreases with growing distance between the facets. Optical power "tunnels" through the gap, establishing a connection with a throughput that depends on the trench width w.

For given slab thickness and material properties, merely three parameters determine the performance of these simple power dividers. Fig. 6 summarizes the dependence of the device reflectance on trench width w, angle of incidence θ, and vacuum wavelength λ, as a basis for an estimation of fabrication tolerances.

In general, the strongest dependence on a deviation of a parameter from its design value is observed for the 3 dB splitters with target level $R = 0.5$. The simulations predict derivatives $\partial_w R = 0.0083/\,\text{nm}$, $\partial_\theta R = 0.037/°$, and $\partial_\lambda R = -0.00048/\,\text{nm}$ for the TE splitter of 60 nm width at $\lambda = 1.55\,\mu$m for incidence at $\theta = 45°$. Likewise, one obtains $\partial_w R = 0.0030/\,\text{nm}$, $\partial_\theta R = 0.028/°$, and $\partial_\lambda R = -0.0017/\,\text{nm}$ for the TM splitter of 211 nm width at $\lambda = 1.55\,\mu$m for incidence at $\theta = 55°$. Material dispersion has been neglected for estimating the wavelength derivative. Note that the wavelength range in Fig. 6(c, f) spans the entire C-band of optical telecommunications. Accepting a linearization as an approximation to the actual parameter dependence, the maximum deviation Δq in a design parameter $q \in \{w, \theta, \lambda\}$ that is permitted for a deviation of no more than ΔR in reflectance can be estimated as $\Delta q = \Delta R/\partial_q R$, where the actual tolerance interval is of width $2|\Delta q|$. What concerns the gap width w, for TE polarization and a deviation in reflectance of ± 0.05, one estimates tolerance intervals of at least 12 nm for all configurations considered. According to Fig. 6(a), the actual intervals are in general not "symmetric" and partly substantially larger than that value. Lower reflectance derivatives indicate larger tolerance intervals for TM polarization.

5 Splitting of semi-guided Gaussian wave bundles

So far we discussed incoming semi-guided plane waves with a single, well-defined angle of incidence, and a strict harmonic y-dependence. In the present context of integrated optics, however, any practically relevant

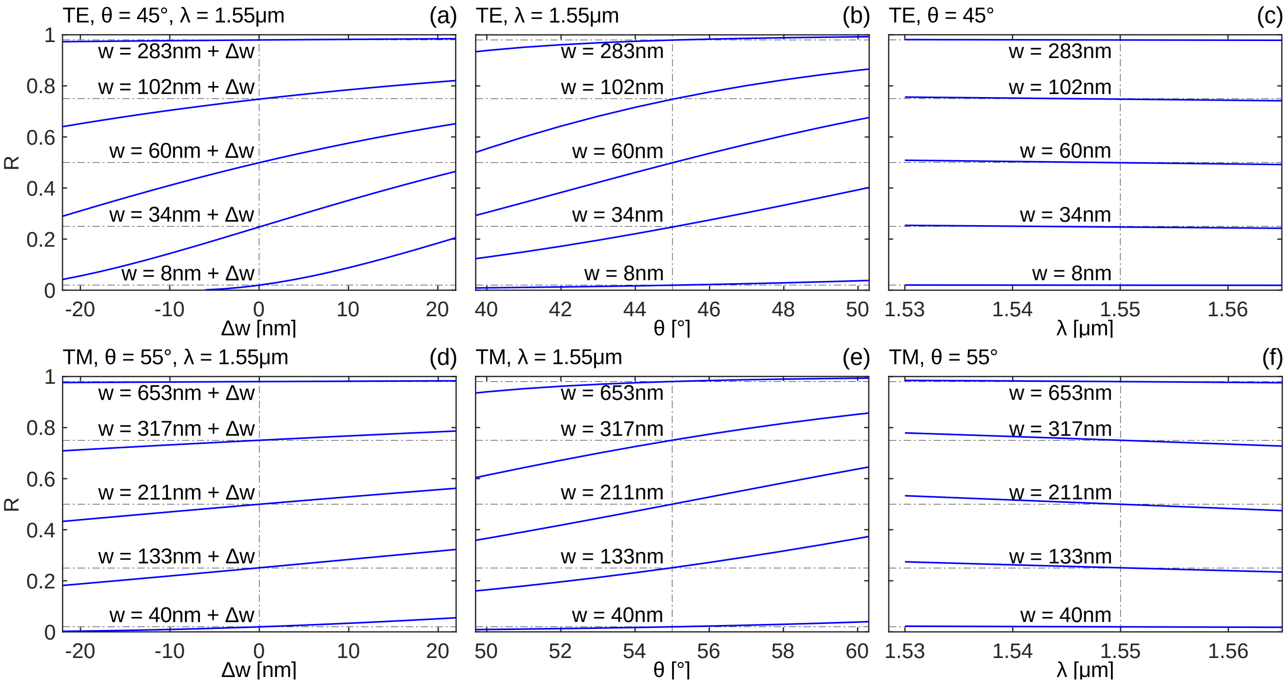

Figure 6: Reflectance R for polarized semi-guided plane waves, coming in at angle θ and vacuum wavelength λ on trenches of width w, dependence of R on variations of either w (a, d), θ (b, e), or λ (c, f).

fields need to be limited in their extension along y. As shown in Refs. [21, 22, 27, 36, 37], this can be achieved by superimposing the former y-infinite solutions with suitable weights over some range of y-wavenumbers, or angles of incidence, respectively. One thus models the oblique incidence of still semi-guided, but now laterally confined "beams". Gaussian superpositions have been considered [21, 27, 36, 37], as well as excitation by incoming rib waveguides with shallow etching [22].

Here we look at TE- or TM-polarized wave bundles with spectrally Gaussian weights. The beams are vertically (x-) guided, in-plane (y, z) of Gaussian shape, focused at the origin $(y, z) = (0, 0)$, and characterized by a primary angle of incidence θ and a beam width W_{b} (full width of the field at focus, in the direction perpendicular to the principal direction of propagation, $1/\mathrm{e}$-level). The quasi-analytical model takes the in-plane beam divergence into account. We refer to [21, 36] for explicit expressions. Fig. 7 illustrates operation of our power dividers for excitation by these beams.

These are non-resonant structures with a moderate dependence of transmission on incidence angle, according to Fig. 6. For Fig. 7 we consider beams with a narrow waist of $W_{\mathrm{b}} = 7\,\mu$m; the divergence of the beams with growing distance from the focus is only just discernible in the figure. Even for these spatially quite narrow beams with their correspondingly wide angular spectral distribution, the power dividers function as predicted for plane wave incidence, up to the given digits for reflectances and transmittances.

6 Trenches of finite length

In case of incidence of semi-guided fields on trenches of finite length, one expects a general distortion of reflected and transmitted waves or wave bundles, edge effects that lead to radiative losses, and correspondingly a change in reflectance and transmittance. For focused incidence and sufficient trench length, however, such that the trench extent covers adequately the lateral tails of the wave bundles, a functioning of the trenches can be expected as predicted for infinite trench length in the former sections. For beams of cross-sectional width W_{b}, incident on a trench at angle θ, the respective beam width W_y in the direction y along the trench is given by $W_y = W_{\mathrm{b}}/\cos(\theta)$. Plots like Fig. 7 can then give hints on the length required for the power dividers.

Note that, for the same principal angle of incidence and for trenches of sufficient lengths, the power transmission characteristics are independent of the position of the beam focus. The values for transmittances and reflectances as given remain constant, irrespective of whether the trench is placed in a converging beam, at the beam focus, or in the diverging beam after the focus. This can be attributed to the orthogonality, in the sense of Fourier-integrals along y, of the exponentials that are superimposed to form the wave bundles [21, 36].

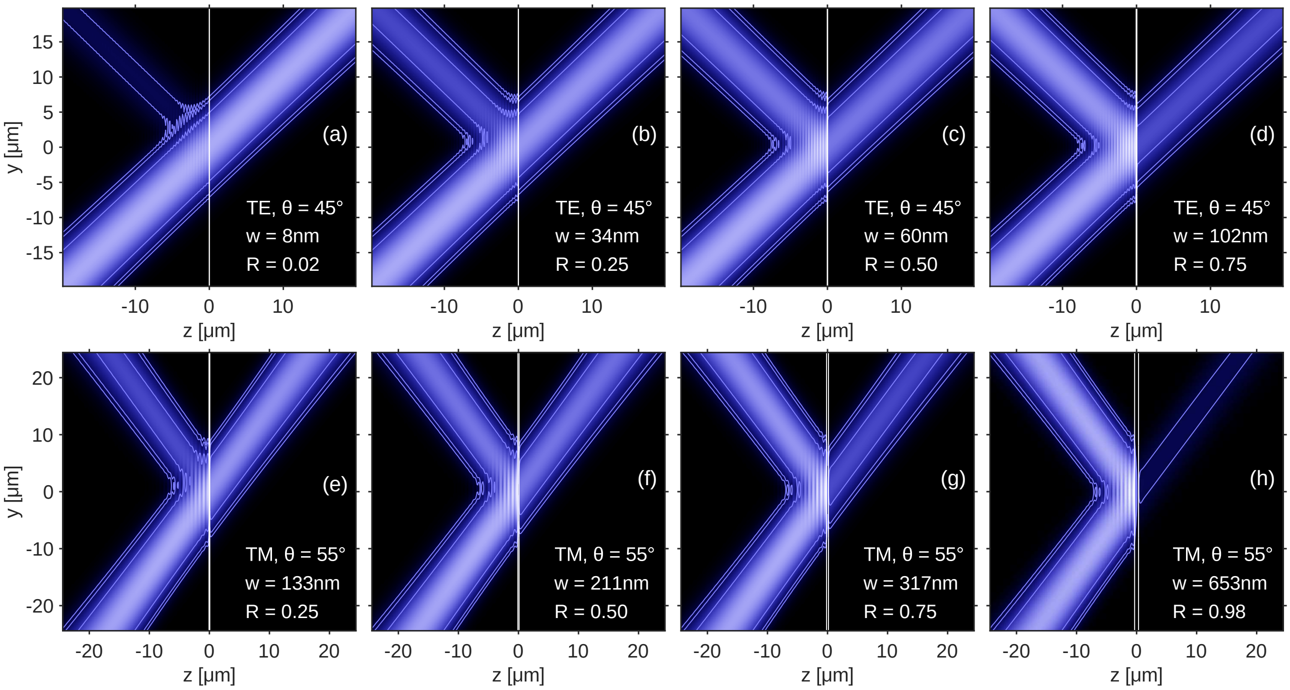

Figure 7: Power dividers of width w, excitation by TE- (a-d) or TM-polarized (e-h) semi-guided Gaussian wave bundles of cross-sectional width $W_b = 7\,\mu m$ at angle θ leads to a reflectance R and transmittance $T = 1 - R$; energy density u of the optical electromagnetic field, contour lines at 5%, 1%, and 0.5% of the maximum level, with a uniform color scale for all panels.

7 1×M-power-divider

The former concept lends itself to cascading. Things become particularly simple in the TE case, with individual splitters operating at an incidence angle of $45°$. As an example, Fig. 8 shows a concept for an $1 \times M$-equal-power divider. The individual trenches are oriented at the $45°$-angle with respect to the axis of the incoming bundle.

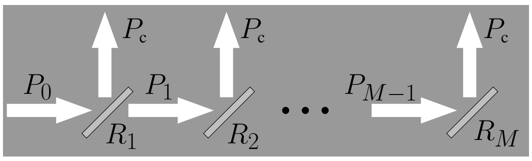

Figure 8: Concept for a $1 \times M$-equal-power divider. A sequence of trenches, each with potentially different width, are arranged along the axis of an incoming semi-guided wave bundle with input power P_0. Each trench with reflectance R_j diverts the power P_c from its input P_{j-1} into one of the M output “channels”.

If one chooses to divide the input power P_0 equally between M outputs, each output channel needs to receive a power of $P_c = P_0/M$. Consequently, the ongoing powers P_j in the sequence should be $P_j = P_{j-1} - P_0/M = P_0(1-j/M)$, and the reflectances of the trenches must be tuned to $R_j = (P_0/M)/P_{j-1}$ or $R_j = 1/(M-j+1)$. Neither resonances nor phase matching mechanisms are involved in this concept. The distance between trenches can be quite arbitrary. As a lower limit, the output beams must not overlap; there are no restrictions on placing trenches further apart, e.g. if required by other circuitry. For narrow beam widths, the divergence of the wave bundles must be considered, though. Obviously, by rotating one of the trenches by $90°$, its output can be directed downward rather than upward.

For the previous analysis, we have chosen the core thickness $d = 0.22\,\mu$m as a standard for silicon photonics thin films. For a larger thickness $d = 0.24\,\mu$m and otherwise unchanged parameters, the slab (still single-mode, but only just) supports a TM mode with larger effective index $N_{TM} = 2.1977$, leading to a lower critical angle for radiative losses $\theta_{b,\,TM} = 41.4°$. Hence, beam splitters for TM modes and TM-$1 \times M$-power dividers could be constructed for the $45°$ angle of incidence just as for TE modes. Different trench widths would be required for operation with TE or TM polarization, though, hence these splitters would not be polarization independent. However, it would just as well be straightforward to construct an $1 \times M$-splitter for TM-polarization with the original thinner films based on the $55°$ incidence angle: The input beam and the array of output beams would then be observed at an angle of $110°$, and perhaps a slightly larger distance between the trenches would be required to avoid overlapping of the output beams.

Note that the design of splitters with arbitrary ratios can be quite involved in a strict waveguide context [4], while here all that is needed is to find adequate trench widths in a figure such as Fig. 4. Tailoring the above multi-output-splitter to other power ratios should thus be straightforward.

8 Polarization beam splitter

Cascading of components, in a regime of small distances, can also lead to promising device concepts [20–22, 30,31]. Likewise, cascading of two of the former trenches can be exploited for the construction of a polarization beam splitter for semi-guided waves. We consider an angle of incidence of $\theta = 55°$, well above the critical angles $\theta_{\rm TE}$, $\theta_{\rm TM}$ for both TE and TM polarization. According to Fig. 4, the TM transmission exceeds the TE transmission for all trench widths w. Hence we aim at a TM-pass polarization splitter, here a configuration with a TE reflectance and a TM transmittance both as close as possible to unity.

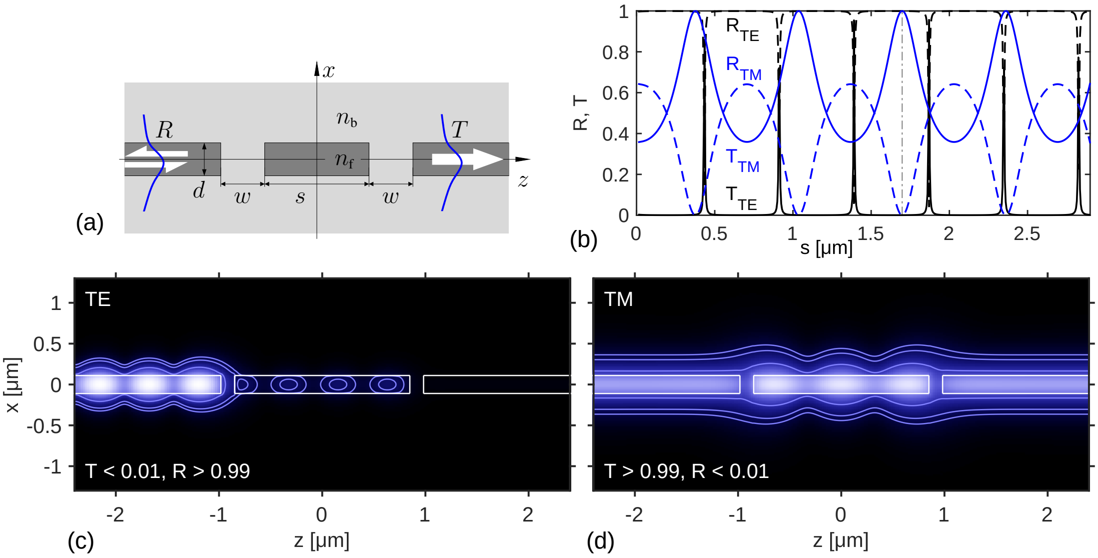

Figure 9: Concept for a polarization beam splitter (a), based on two trenches of width w at a distance s; all other parameters are as given for Fig. 1. (b) Reflectance R (dashed) and transmittance T (continuous) versus the distance s, for TE and TM excitation at $\theta = 55°$, for $w = 133$ nm. (c, d) energy-density u on the x-z-plane for the splitter with separation $s = 1.698\,\mu$m, for TE (c) and TM input (d).

A possible design uses two identical power dividers, as shown in Fig. 9(a). For the moment we adopt a view of 1-D wave propagation in $\pm z$-direction. The trenches then act as identical partial reflectors, that establish resonances of Fabry-Perot-type, i.e. realize states of full transmission, for certain distances s between the reflectors. The reflectances associated with the trenches, and consequently also the shape / linewidth (vs. s) of the transmission resonances, differ for TE and TM polarization.

Rather arbitrarily we fix a width $w = 133$ nm that effects, for an individual trench, a larger reflectance $R_{\rm TE} = 0.96$ for TE waves, and only a moderate level $R_{\rm TM} = 0.25$ for TM fields. As shown in Fig. 9(b), for the composite system this leads to T, R vs. s -curves with narrow transmission peaks for TE input, with “flat” regions of high TE reflectance in-between, while the TM transmission resonances are rather wide and largely overlapping. These features repeat with a certain periodicity: In any homogeneous region of the slab, a mode with effective index N, propagating at angle θ with respect to the z-direction with wavenumber $k_z = kN\cos\theta$, relates to a field with spatial periodicity along z with a period $\Lambda_z = \lambda/(N\cos\theta)$. At $\theta = 55°$, one obtains $\Lambda_{z,\rm TE} = 0.957\,\mu$m and $\Lambda_{z,\rm TM} = 1.325\,\mu$m for TE and TM polarization, respectively. Standard Fabry-Perot theory then predicts that states with full transmission occur periodically in s, with a period of $\Delta s = \Lambda_z/2$, as it is confirmed by Fig. 9(b).

Due to the comparably large difference in the periods, a reasoning in terms of a beat length to identify a distance s, that is suitable for a polarization splitter, is not really useful here. It suffices to just look up a value s, where a TM transmission resonance appears within a flat-top TE reflectance maximum. The thin dash-dotted vertical line in Fig. 9(b) at $s = 1.698\,\mu$m indicates a distance, for which both the TE reflectance and the TM transmittance of the device deviate from unity by less than 1%. Panels (c, d) of Fig. 9 show the cross-sectional fields.

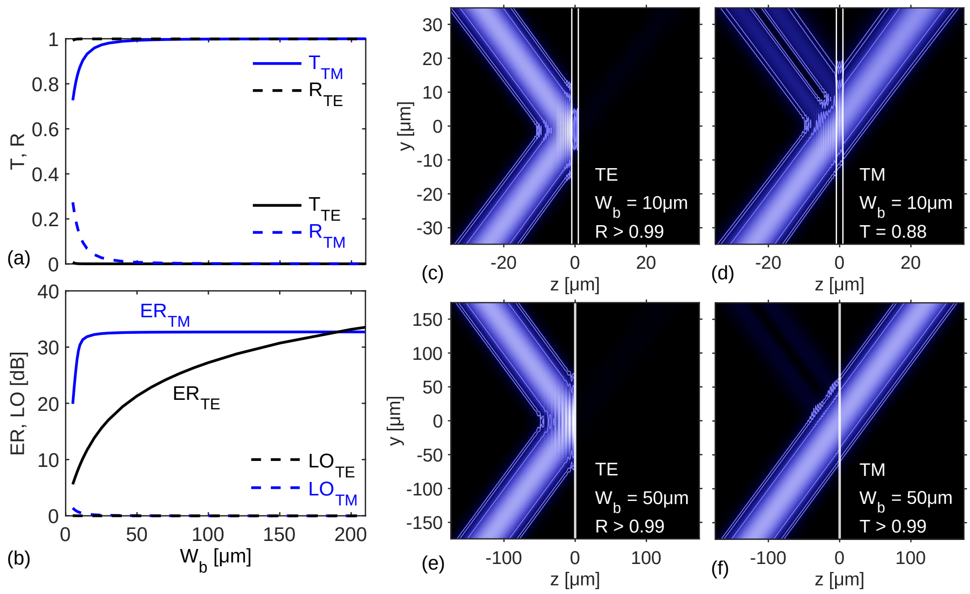

Figure 10: Excitation of the polarization beam splitter of Fig. 9 by semi-guided Gaussian beams, transmittance T and reflectance $R = 1 - T$ (a), and extinction ratios ER and insertion loss LO (b), for TE- and and TM-input, as a function of the beam width W_b. (c)–(f): Energy density u of the optical electromagnetic field for incoming beams of width $W_b = 10\,\mu$m (c, d) and $W_b = 50\,\mu$m (e, f), contour lines at 5%, 1%, and 0.5% of the maximum level; all panels use the same color scale. Parameters $\theta = 55°$ (principal angle), $w = 133$ nm, $s = 1.698\,\mu$m are as given for Fig. 9(c, d).

Finally we briefly consider the focused excitation of the polarization splitter. Fig. 10 compares results for different beam widths W_b. By construction, the incident light bundles contain waves at a range of angles around the principal beam angle θ. The angular response of the device, for oblique plane wave incidence (not shown), exhibits a resonant behavior of certain widths for TE- and TM-polarization, with good or optimum values at the design angle of $55°$. Apparently, for the narrower beams of width $W_b = 10\,\mu$m, not all components of the wider angular distribution are captured by the TM transmission resonance, such that the transmittance is lower than that for semi-guided plane wave incidence in Fig. 9(d). For wider input beams with narrower angular distributions, as well as for TE polarization (off-resonance operation), the polarization beam splitter performs comparably for focused and for plane-wave incidence. More specifically, for beam width $W_b = 10\,\mu$m, one could characterize the device as a TM-pass polarizer with an extinction ratio $\mathrm{ER}_{\mathrm{TM}} = 10\log_{10}(T_{\mathrm{TM}}/T_{\mathrm{TE}}) = 30.4$ dB and an insertion loss $\mathrm{LO}_{\mathrm{TM}} = -10\log_{10}(T_{\mathrm{TM}}) = 0.58$ dB. At bundle width $W_b = 50\,\mu$m, the polarization beam splitter reaches levels of $\mathrm{ER}_{\mathrm{TM}} = 32.6$ dB and $\mathrm{LO}_{\mathrm{TM}} = 0.03$ dB for the TM path, and an extinction ratio $\mathrm{ER}_{\mathrm{TE}} = 10\log_{10}(R_{\mathrm{TE}}/R_{\mathrm{TM}}) = 21.3$ dB and loss $\mathrm{LO}_{\mathrm{TE}} = -10\log_{10}(R_{\mathrm{TE}}) = 0.003$ dB for the TE path. According to Fig. 10(a, b), these values improve even further for wider beams; also a re-design with modified starting values for the width w and angle of operation θ might lead to further optimization.

9 Concluding remarks

Simple rectangular trenches in a high-index slab can act as power dividers for polarized semi-guided waves, harnessing the mechanism of frustrated total internal reflection. The devices are easily configurable for the full range of splitting ratios $[0, 1]$. Neither resonances nor phase-matching arguments play a role, therefore the power dividers are comparably broadband. For a 3 dB splitter designed for TE operation at $1.55\,\mu$m wavelength, we calculated at maximum deviation in reflectance of ± 0.008 over the entire telecom-C-band. Assuming that material attenuation and surface roughness can be neglected, the splitters are lossless. Straightforward cascading opens up possibilities for other types of power dividers, e.g. with multiple outlets. We have evaluated a simple design for a polarization beam splitter that relies on resonances of Fabry-Perot-type, established by two of the former power dividers.

The required chip surface is largely determined by the lateral width of the semi-guided beams with which the devices operate. In general, this size will be considerably larger than what can be achieved in a context of conventional high-contrast single-mode waveguides ("wires") of silicon photonics. Still, sidewall roughness is among the major sources of optical power loss in many integrated optical systems. Devices that operate on the present beams of semi-guided waves might be able to largely avoid these losses [19]: For the power dividers discussed in this paper, etching-roughness-related losses would arise from the trench flanks only, not from the long propagation distances in between devices. This might be relevant in fields like single-photon processing in quantum optics [50, 51], where prevention of losses is of particular importance, or in a field where devices are of a substantial size anyway, e.g. to exploit nonlinear effects.

A Nonsymmetric slab waveguides

Among the devices for semi-guided waves listed at the beginning of Section 2, many — not all — of the concepts concern structures based on high-index silicon films on oxide substrates or buffers, covered by air. For the beam splitters to become compatible, we thus look briefly at the changes in the former theory as required for these nonsymmetric host waveguides.

As before we consider parameters for silicon slabs with refractive index $n_{\rm f} = 3.45$ of "standard" thickness $d = 0.22\,\mu$m on a silica substrate / buffer ($n_{\rm s} = 1.45$), now with an air cover ($n_{\rm c} = 1.0$), at a vacuum wavelength $\lambda = 1.55\,\mu$m. These waveguides support fundamental TE and TM modes with effective indices $N_{\rm TE} = 2.8051$ and $N_{\rm TM} = 1.8748$ which are slightly lower than those in the former symmetric waveguides. This leads to higher critical angles $\theta_{\rm s,TE} = 31.1°$ and $\theta_{\rm s,TM} = 50.7°$ for radiative losses in the substrate. Losses due to radiation into the air cover are suppressed for incidence at angles above $\theta_{\rm c,TE} = 20.9°$ and $\theta_{\rm c,TM} = 32.2°$, respectively. Further, a critical angle $\theta_{\rm TM,TE} = 41.9°$ limits the range where an incoming TE polarized wave can excite reflected or transmitted TM waves. Conversely, with effective indices $N_{\rm TE} > N_{\rm TM}$, there is no such angle for the conversion from TM to TE: Coupling from an incoming TM mode to reflected or transmitted TE waves is possible for the entire $[0, 90]°$-range of incidence angles.

The dependence of reflectance and transmittance on the trench width w is key for the design of the power dividers. Fig. 11 shows respective plots for nonsymmetric access waveguides. Panels (a) and (b) correspond to a trench structure with air gap; for (c) and (d) the trench is assumed to be filled with the substrate medium. The curves are to be compared to those in Fig. 4 for the symmetric waveguides.

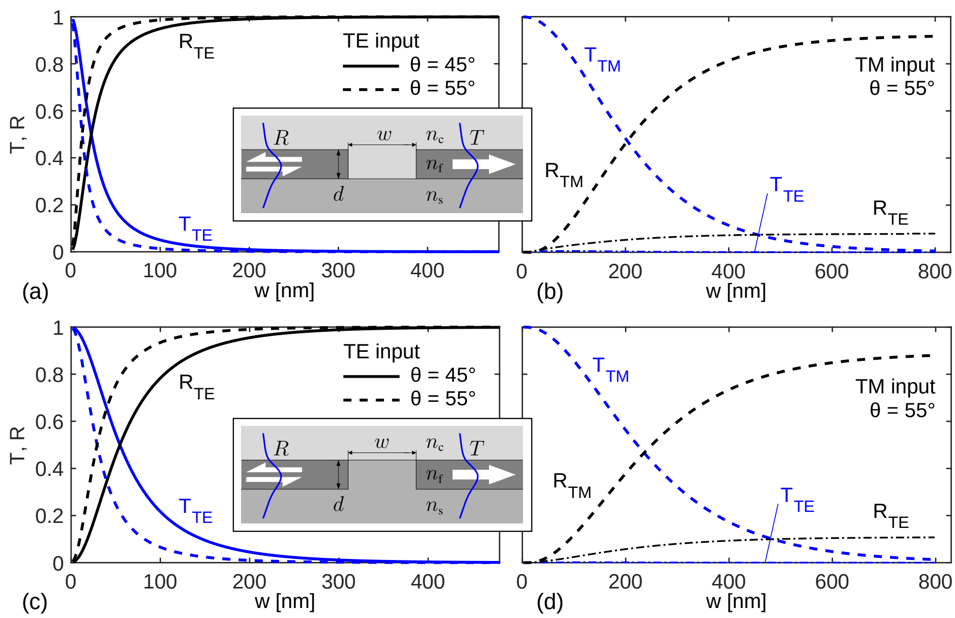

Figure 11: Oblique incidence of semi-guided waves on trench structures with nonsymmetric layering, with refractive indices $n_s : n_f : n_c = 1.45 : 3.45 : 1.0$ and air gap (a, b), and a filled trench (c, d). Reflectance R and transmittance T versus the trench width w, curves for TE (a, c) and TM excitation (b, d), at angles $\theta = 45°$ (continuous) and $\theta = 55°$ (dashed, dash-dotted).

We start with the results for TE excitation of air trenches in panel Fig. 11(a). When compared to the symmetric case, the larger refractive index contrast $n_{\rm f} : n_{\rm c}$ across the trench sidewalls causes a more rapid decay of the field in the gap, and correspondingly a steeper slope of the reflectance and transmittance curves. Lossless TE-power-dividers with the full 0-to-1-range of reflectance are still feasible, in principle. However, this requires the realization of narrower gaps with prospectively stricter tolerances. According to panel (c), these constraints relax for trenches filled with a higher index medium. In that case, the construction of single splitters and combined devices for TE operation should be possible just as for the symmetric waveguides.

Things change for excitation by TM modes, as seen in Fig. 11(b, d). The change in the curves' slope for air-filled trenches is less pronounced than for TE polarization. One observes a noticeable polarization conversion, with levels of TM-to-TE power transfer of about 8% (air gap) and 10% (filled trenches), mainly to the reflected TE mode. Radiative losses are still suppressed, in the sense that the reflectances and transmittances for the fundamental guided TE- and TM-modes add up to unity. If TM-only operation is required, however, with $R_{\mathrm{TM}} + T_{\mathrm{TM}} < 1$ these trenches can no longer be regarded as lossless devices. Trenches of large width still work as mirrors that reflect the full input power; these are not polarization maintaining mirrors that convert about $8\% / 10\%$ of the TM input to TE. Hence it depends on the particular application, whether the trenches in nonsymmetric slabs can be serviceable.

We conclude that, in general, the oxide cover is beneficial for the beam splitter design. Where perhaps some of the concepts for other devices might also be adaptable to an oxide cover, or a cover layer could be required for some composite circuit for entirely different reasons.

A.1 Slanted trench sidewalls

Even for the symmetric setting with oxide cover, fabrication processes could result in trenches with slanted sidewalls, i.e. could break the overall symmetry. Qualitatively, we expect two different effects. On the one hand, for given gap width, trench flanks at oblique angles would result in a modified "tunnelling strength" of the field, when compared to the vertical flanks, with different reflectance. If the sidewall angle would be known for a particular process, this could be easily incorporated in the simulations (though not with the semi-analytical tools used in this paper, which rely on a rectangular geometry; numerical simulations could be carried out alternatively, as in Ref. [22]). The design values for the gap widths could then be corrected accordingly. On the other hand, the violation of the vertical symmetry could lead to polarization coupling, similar to the features seen for the nonsymmetric structure in the first part of this section. Further numerical simulations offer a way to assess the effect, in case that is deemed necessary.

Funding

Financial support from the German Research Foundation (Deutsche Forschungsgemeinschaft DFG, project 231447078–TRR 142, subproject C05) is gratefully acknowledged.

Disclosures

The authors declare no conflicts of interest.

Data availability

Data underlying the results presented in this paper are not publicly available at this time but may be obtained from the authors upon reasonable request.

References

[1] J. Zhu, Q. Chao, H. Huang, Y. Zhao, Y. Li, L. Tao, X. She, H. Liao, R. Huang, Z. Zhu, X. Liu, Z. Sheng, and F. Gan. Compact, broadband, and low-loss silicon photonic arbitrary ratio power splitter using adiabatic taper. *Applied Optics*, 60(2):413–416, 2021.

[2] T. Lunghi, F. Doutre, A. P. Rambu, M. Bellec, M. P. De Micheli, A. M. Apetrei, O. Alibart, N. Belabas, S. Tascu, and S. Tanzilli. Broadband integrated beam splitter using spatial adiabatic passage. *Optics Express*, 26(21):27058–27063, 2018.

[3] B. I. Akca, B. Považay, A. Alex, K. Wörhoff, R. M. de Ridder, W. Drexler, and M. Pollnau. Miniature spectrometer and beam splitter for an optical coherence tomography on a silicon chip. *Optics Express*, 21(14):16648–16656, 2013.

[4] K. Xu, L. Liu, X. Wen, W. Sun, N. Zhang, N. Yi, S. Sun, S. Xiao, and Q. Song. Integrated photonic power divider with arbitrary power ratios. *Optics Letters*, 42(4):855–858, 2017.

[5] E. Eyal Terkieltaub-Lee, Y. Albeck, and A. Karsenty. Mode analysis and optimization of split Y-junction sharing very low index difference. *Journal of Nanophotonics*, 13(2):1–12, 2019.

[6] R. Halir, A. Ortega-Monux, D. Benedikovic, G. Z. Mashanovich, J. G. Wanguemert-Perez, J. H. Schmid, I. Molina-Fernandez, and P. Cheben. Subwavelength-grating metamaterial structures for silicon photonic devices. *Proceedings of the IEEE*, 106(12):2144–2157, 2018.

[7] S. Zhu. Ultra-broadband and ultra-compact polymer waveguide polarization beam splitter using a T-junction with obliquely embedded subwavelength gratings. *Microprocessors and Microsystems*, page 103947, 2021.

[8] X. Liu, D. Liu, and D. Dai. Silicon polarization beam splitter at the 2 μm wavelength band by using a bent directional coupler assisted with a nano-slot waveguide. *Optics Express*, 29(2):2720–2726, 2021.

[9] Y. Zhang, Y. He, J. Wu, X. Jiang, R. Liu, C. Qiu, X. Jiang, J. Yang, C. Tremblay, and Y Su. High-extinction-ratio silicon polarization beam splitter with tolerance to waveguide width and coupling length variations. *Optics Express*, 24(6):6586–6593, 2016.

[10] B. Shen, P. Wang, and R. Polson. An integrated-nanophotonics polarization beamsplitter with 2.4$\times$2.4 μm footprint. *Nature Photonics*, 9:378–382, 2015.

[11] D. Pérez-Galacho, R. Halir, A. Ortega-Moñux, C. Alonso-Ramos, R. Zhang, P. Runge, K. Janiak, H.-G. Bach, A. G. Steffan, and Í. Molina-Fernández. Integrated polarization beam splitter with relaxed fabrication tolerances. *Optics Express*, 21(12):14146–14151, 2013.

[12] F. Çivitci, M. Hammer, and H. J. W. M. Hoekstra. Semi-guided plane wave reflection by thin-film transitions for angled incidence. *Optical and Quantum Electronics*, 46(3):477–490, 2014.

[13] M. Hammer, L. Ebers, A. Hildebrandt, S. Alhaddad, and J. Förstner. Oblique semi-guided waves: 2-D integrated photonics with negative effective permittivity. In *2018 IEEE 17th International Conference on Mathematical Methods in Electromagnetic Theory (MMET)*, pages 9–15, 2018.

[14] R. Soref. The past, present, and future of silicon photonics. *IEEE Journal of Selected Topics in Quantum Electronics*, 12(6):1678–1687, 2006.

[15] E. Hecht. *Optics*. Pearson Education, 2017.

[16] R. Ulrich and R. J. Martin. Geometrical optics in thin film light guides. *Applied Optics*, 10(9):2077–2085, 1971.

[17] P. K. Tien, S. Riva-Sanseverino, R. J. Martin, and G. Smolinsky. Two-layered construction of integrated optical circuits and formation of thin-film prisms, lenses, and reflectors. *Applied Physics Letters*, 24(11):547–549, 1974.

[18] P. K. Tien. Integrated optics and new wave phenomena in optical waveguides. *Reviews of Modern Physics*, 49(2):361–419, 1977.

[19] W. P. Tresna, A. W. S. Putra, and T. Maruyama. Optical-loss measurement of a silicon-slab waveguide. *Current Optics and Photonics*, 4(6):551–557, 2020.

[20] M. Hammer, A. Hildebrandt, and J. Förstner. How planar optical waves can be made to climb dielectric steps. *Optics Letters*, 40(16):3711–3714, 2015.

[21] M. Hammer, A. Hildebrandt, and J. Förstner. Full resonant transmission of semi-guided planar waves through slab waveguide steps at oblique incidence. *Journal of Lightwave Technology*, 34(3):997–1005, 2016.

[22] L. Ebers, M. Hammer, and J. Förstner. Oblique incidence of semi-guided planar waves on slab waveguide steps: Effects of rounded edges. *Optics Express*, 26(14):18621–18632, 2018.

[23] M. Hammer, L. Ebers, and J. Förstner. Oblique quasi-lossless excitation of a thin silicon slab waveguide: a guided-wave variant of an anti-reflection coating. *Journal of the Optical Society of America B*, 36(9):2395–2401, 2019.

[24] M. Hammer, L. Ebers, and J. Förstner. Optischer Übergang zwischen zwei optischen Schichtwellenleitern und Verfahren zum Übertragen von Licht. German Patent DE 10 2018 108 110 B3, Deutsches Patent- und Markenamt (filed 05.04.2018, issued 31.01.2019).

[25] E. A. Bezus, D. A. Bykov, and L. L. Doskolovich. Bound states in the continuum and high-Q resonances supported by a dielectric ridge on a slab waveguide. *Photonics Research*, 6(11):1084–1093, 2018.

[26] L. L. Doskolovich, E. A. Bezus, and D. A. Bykov. Two-groove narrowband transmission filter integrated into a slab waveguide. *Photonics Research*, 6(1):61–65, 2018.

[27] E. A. Bezus, L. L. Doskolovich, D. A. Bykov, and V. A. Soifer. Spatial integration and differentiation of optical beams in a slab waveguide by a dielectric ridge supporting high-Q resonances. *Optics Express*, 26(19):25156–25165, 2018.

[28] M. Hammer, L. Ebers, and J. Förstner. Oblique evanescent excitation of a dielectric strip: A model resonator with an open optical cavity of unlimited Q. *Optics Express*, 27(7):9313–9320, 2019.

[29] T. G. Nguyen, G. Ren, S. Schoenhardt, M. Knoerzer, A. Boes, and A. Mitchell. Ridge resonance in silicon photonics harnessing bound states in the continuum. *Laser & Photonics Reviews*, 13(10):1900035, 2019.

[30] T. G. Nguyen, K. Yego, G. Ren, A. Boes, and A Mitchell. Microwave engineering filter synthesis technique for coupled ridge resonator filters. *Optics Express*, 27(23):34370–34381, 2019.

[31] L. L. Doskolovich, E. A. Bezus, and D. A. Bykov. Integrated flat-top reflection filters operating near bound states in the continuum. *Photonics Research*, 7(11):1314–1322, 2019.

[32] D. A. Bykov, E. A. Bezus, and L. L. Doskolovich. Bound states in the continuum and strong phase resonances in integrated gires-tournois interferometer. *Nanophotonics*, 9(1):83–92, 2020.

[33] E. A. Bezus, D. A. Bykov, and L. L. Doskolovich. Integrated gires–tournois interferometers based on evanescently coupled ridge resonators. *Optics Letters*, 45(18):5065–5068, 2020.

[34] S. Schoenhardt, A. Boes, T. G. Nguyen, and A. Mitchell. Ridge resonators: impact of excitation beam and resonator losses. *Optics Express*, 29(17):27092–27103, 2021.

[35] M. Hammer, L. Ebers, and J. Förstner. Hybrid coupled mode modelling of the evanescent excitation of a dielectric tube by semi-guided waves at oblique angles. *Optical and Quantum Electronics*, 52:472, 2020.

[36] M. Hammer, L. Ebers, and J. Förstner. Resonant evanescent excitation of guided waves with high-order optical angular momentum. *Journal of the Optical Society of America B*, 38(5):1717–1728, 2021.

[37] L. Ebers, M. Hammer, and J. Förstner. Light diffraction in slab waveguide lenses simulated with the stepwise angular spectrum method. *Optics Express*, 28(24):36361–36379, 2020.

[38] F. Çivitci, M. Hammer, and H. J. W. M. Hoekstra. Planar prism spectrometer based on adiabatically connected waveguiding slabs. *Optics Communications*, 365:29–37, 2016.

[39] R. Wang, J. Chen, Y. Xiang, Y. Kuai, P. Wang, H. Ming, J. R. Lakowicz, and D. Zhang. Two-dimensional photonic devices based on Bloch surface waves with one-dimensional grooves. *Physical Review Applied*, 10:024032, 2018.

[40] A. Hadij-ElHouati, P. Cheben, A. Ortega-Moñux, J. G. Wangüemert-Pérez, R. Halir, J. de Oliva-Rubio, J. H. Schmid, and I. Molina-Fernández. High-efficiency conversion from waveguide mode to an on-chip beam using a metamaterial engineered Bragg deflector. *Optics Letters*, 46(10):2409–2412, 2021.

[41] M. L. Dakss, L. Kuhn, P. F. Heidrich, and B. A. Scott. Grating coupler for efficient excitation of optical guided waves in thin films. *Applied Physics Letters*, 16(12):523–525, 1970.

[42] D. Taillaert, P. Bienstman, and R. Baets. Compact efficient broadband grating coupler for silicon-on-insulator waveguides. *Optics Letters*, 29(23):2749–2751, 2004.

[43] M. Hammer. Oblique incidence of semi-guided waves on rectangular slab waveguide discontinuities: A vectorial QUEP solver. *Optics Communications*, 338:447–456, 2015.

[44] M. Hammer. OMS — 1-D mode solver for dielectric multilayer slab waveguides. http://www.computational-photonics.eu/oms.html.

[45] I. V. Lindell and A. H. Sihvola. Electromagnetic boundary conditions defined in terms of normal field components. *IEEE Transactions on Antennas and Propagation*, 58(4):1128–1135, 2010.

[46] M. Hammer. Quadridirectional eigenmode expansion scheme for 2-D modeling of wave propagation in integrated optics. *Optics Communications*, 235(4–6):285–303, 2004.

[47] M. Hammer. METRIC — Mode expansion tools for 2D rectangular integrated optical circuits. http://metric.computational-photonics.eu/.

[48] M. Born and E. Wolf. *Principles of Optics, 7th. ed.* Cambridge University Press, Cambridge, UK, 1999.

[49] M. Hammer. MULS — Oblique incidence of plane waves on dielectric multilayer stacks. http://www.computational-photonics.eu/muls.html.

[50] D. F. Walls and G. J. Milburn. *Quantum optics*. Springer-Verlag, Berlin, Heidelberg, 2008.

[51] D. Bonneau, G. J. Mendoza, J. L. O'Brien, and M. G. Thompson. Effect of loss on multiplexed single-photon sources. *New Journal of Physics*, 17(4):043057, 2015.